A comprehensive control strategy for integrated flight/propulsion systems

M Yasar[1], A Ray[1]*, and J F Horn[2]

[1]Mechanical Engineering Department, The Pennsylvania State University, University Park, Pennsylvania, USA

[2]Aerospace Engineering Department, The Pennsylvania State University, University Park, Pennsylvania, USA

Abstract: Integration of flight and propulsion control systems in advanced aircraft has attracted much attention because of ever increasing demand on enhancement of performance and reliability. As the underlying dynamic couplings and non-linear interactions of flight and propulsion systems are too complex for realtime execution in onboard computational platforms, hierarchical hybrid (i.e. combined continuously varying and discrete event) architecture is proposed for the development of future generation control systems that will take the advantage of these interactions for mission enhancement. Although the original structures of continuously varying control systems for propulsion and flight are retained, discrete event supervisory (DES) control would facilitate decision-making for aircraft operation. DES decisions regarding propulsion and flight control influence the performance and reliability of the entire vehicle control system due to interactions at the level of continuously varying dynamics. A two-level hierarchical DES control system is designed to supervise and coordinate the operation of twin-engine aircraft propulsion with flight dynamics. In essence, the propulsion system is integrated with the flight dynamical system such that the DES controller at the propulsion level of hierarchy provides load balancing of the engines as well as overall health and mission management of the aircraft propulsion system. The parameter-scheduling dynamic-inversion controller stabilizes and drives the flight system in the vehicle operation envelope and compensates for potential unbalance and any other undesirable action, resulting from discrete event supervision of the propulsion system. Results of real-time simulation on a test bed are presented to demonstrate the efficacy of the proposed control concept.

Keywords: integrated flight/propulsion, supervisory control, discrete event systems, dynamic inversion

1 INTRODUCTION

Development of intelligent decision and control algorithms based on the theory of discrete event supervisory (DES) control [1, 2] has paramount importance in many military and commercial applications. Especially, as interactions among complex systems may not be adequately described solely through an understanding of individual component's dynamics, human reasoning, and tools of artificial intelligence are often applied for modelling and control of such integrated systems. For example, mission and vehicle operation management systems and military command, control, communications, computer, intelligence, surveillance, and reconnaissance (C^4ISR) systems belong to the class of discrete event systems, where the evolution of the temporal behaviour depends on the complex interactions among various discrete events, such as initiation or completion of operations and success or failure of certain missions. The algorithms for DES control synthesis have evolved based on automata theory and formal languages [1, 3, 4].

Recent theoretical developments [4–6] in the DES control theory have led to several applications in the aerospace field [7–9]. These applications are largely

Corresponding author: Department of Mechanical Engineering, Pennsylvania State University, 329 Reber Building, University Park, PA 16802, USA. email: axr2@psu.edu

confined to interactions between the DES control module and the continuous-time plant under discrete event supervision. Consequently, the resulting DES control policies can be implemented without considering dynamical effects of the supervisory decisions on other continuous-time systems, which are coupled with the DES controlled plant.

This paper addresses intelligent decision and control of a twin-engine aircraft propulsion system, where a hierarchical structure is employed in the following sense: continuously varying control of each engine [10] interacts with its own local DES controller for health monitoring and life extending control [11, 12]. The operational information is abstracted and reported to the coordinator for propulsion-level DES control of both engines [9]. The DES controller, reported in this paper, provides load balancing between the twin engines under various operating conditions. It is important to note that load distribution of the engines has a significant impact on both flight dynamics and engine dynamics.

The effects of dynamic coupling between the engine model and flight model may not be clearly understood unless these two systems are examined together [13]. For a given input throttle position, the effects of coupling between altitude and Mach number cannot be ignored. Recently, Yasar and Ray [9] have reported DES control of aircraft propulsion systems for intelligent decision-making regarding engine health monitoring and load balancing to provide a baseline for the design of aircraft control systems; however, this study did not address the effects of coupling between the engine and flight parameters. Integration of flight and propulsion systems has been studied by several researchers [14–16] to take advantage of favourable interactions as well as to mitigate the effects of adverse interactions between the two systems. In these studies, the available flight system models incorporated simplified engine models, consisting of only static functions and tabulated thrust values adjoined with low-order linear dynamics. In order to study the interacting effects where propulsion is directly involved in controlling the aircraft, it is essential that the non-linear dynamic response of the engines be adequately modelled [17–19].

Above discussions evince that it is logical to combine the DES decision and control of the propulsion system with the flight control system to enhance the interactions between propulsion dynamics and aerodynamics. It is also imperative to show that the propulsion-level supervisor is not affected adversely from the coupling between engine and flight dynamics. The objectives of this paper are:

(a) observation of the effects of supervisory decisions (at the propulsion level) on the aerodynamic control surfaces;

(b) construction of a comprehensive control architecture to stabilize and drive the integrated system while the plant's operational behaviour is supervised in the discrete event setting.

A linear model-inverting architecture [20] is incorporated to stabilize the aircraft by adjusting the control surfaces to offset the possible adverse effects of discrete event supervision.

This paper is organized in six sections, including the present one, and two appendices that provide supporting information on both engine dynamics and flight dynamics. In section 2, the engine model and the supervisory decisions for propulsion control are reviewed along with the supporting information in Appendix 2. Section 3 along with the supporting information in Appendix 3 introduces the flight dynamic model and describes integration of the flight and propulsion system models. Section 4 presents the parameter-scheduling dynamic-inversion control law. The results of simulation on a networked test bed of aircraft flight and propulsion are presented and discussed in section 5. The paper is summarized and concluded in section 6. Appendix 2 provides pertinent equations for an analytical model of engine operations. Appendix 3 lists the governing equation of flight operations based on the principles of rigid-body dynamics.

2 ENGINE MODEL AND SUPERVISORY CONTROL

This section presents the features of a generic gas turbine engine model employed as the plant for (DES) control of the propulsion system as well as for supervisory decision-making in health monitoring and life extending control [11, 12]. The engine model is similar in complexity and details to that reported by Diao and Passino [21] and modular aero propulsion system simulation model of NASA [22]. Appendix 2 lists pertinent governing equations of the engine simulation model.

Given the inputs of throttle position, also known as power lever angle (PLA), and ambient conditions (e.g. altitude (h), Mach number (M), ambient temperature (T_a)), non-linear dynamics of turbofan engine dynamics are represented as a component level model. Both steady-state and transient operations of the gas turbine engine are simulated in the continuous-time setting.

A typical high-pressure ratio, dual-spool, low bypass, gas turbine engine is represented with a non-linear, low bandwidth, performance model, which is used in applications of intelligent engine control. The components of this engine model consist of a single-stage high-pressure ratio fan with variable inlet stator vanes, booster with independent hub and tip stator vanes, high-pressure mixed flow compressor,

double-annular combustor, high- and low-pressure turbines, afterburner, and nozzle components [22, 23]. The open-loop engine model has three state variables, which are the low-pressure and the high-pressure rotor speeds, as well as the average metal (wall) temperature. Together with its ten actuators, the total number of states associated with the augmented plant model is 23.

The DES control law has been tested on a networked test bed that simulates dynamic flight and propulsion conditions. The network consists of four computers communicating via a network hub, three of which host the continuously varying plants and DES control units, the other is the pilot station. The plant dynamics in the simulation test bed are built upon the model of a generic turbofan gas turbine engine and a generic fighter aircraft model. The software architecture of the test bed is flexible to adapt piloted and autonomous flights with open-source flight simulator programme FlightGear [24]. The DES system treats the engine model together with its continuously varying multi-variable controller as the plant for open-loop (i.e. unsupervised) discrete event behaviour. The continuous-time gain-scheduling robust controller of the turbofan engine is kept unaltered in the DES control system. Details of the hierarchical DES control system, including its optimization and implementation, have been recently reported by Yasar and Ray [9].

Regarding the engine operation, there are two types of possible supervisory decisions in the present architecture. Examples of local supervisory decisions are adjustments in engine actuator commands and changes in distribution of thrust demands from the engines. As reported in the previous work [9], the local supervisor acts as a decision maker for actuator positions under the thrust demand coming from propulsion-level supervisor while limiting the component damage. Figure 1(a) exhibits excessive oscillations in the engine thrust for operation at an elevated throttle position without DES control. As seen in Fig. 1(b), these oscillations are stabilized by DES control in the following way.

The local DES controller decides to reduce the variable nozzle area of the engine by 20 per cent upon the detection of high-frequency instabilities in combustor temperature and high-pressure turbine speed. High-frequency oscillations of temperature and pressure are considered as the primary cause for structural damage in the turbine blades and hence degradation of the engine health. A comparison of the engine performance profiles in the two plates of Fig. 1 indicates that the instabilities are quenched in less than 1 min by reducing the nozzle area, which is implemented as an additional input signal to the (electronic) summation junction in the actuator control software. In this way, the control law and the control command are left unaltered.

If the ultimate decisions for mission-related operations are solely made by the pilot, the propulsion-level DES controller could behave in a decision support role for critical decisions (e.g. mission abortion). The other regulation imposed by the propulsion-level supervisor (that also acts as a risk assessment unit for health management of the propulsion system) is based on the load entrusted to each engine [9]. Making use of the analytical tools developed for anomaly detection [25], the propulsion-level supervisor decides on the health conditions of individual engines and determines the thrust demand levels for the local supervisors. The issue of load balancing becomes important when the health of two engines are significantly different. For example, one engine could be in 'bad health' whereas the other is in 'good health'. In this situation, the DES controller aims at redistribution of the total thrust between two engines such that the 'unhealthy' engine carries lower load than the 'healthy' one. The goal of the thrust redistribution scheduled in the DES is to maintain the total thrust output unaltered while ensuring the safe operating condition that is subject to the constraint of not exceeding the maximum allowable differential thrust. Simulation experiments on the test bed have been conducted for load distribution of 55 and 45 per cent for healthy and unhealthy engines, respectively.

Load distribution can be achieved through either an outer feedback loop over the existing engine controller or a feedforward structure. For the feedback loop, a proportional and integral control is designed to track the reference thrust value, which is 45 or 55 per cent of the total produced thrust just before load redistribution is enforced depending on the health condition of the engine. In contrast, a proportional control is sufficient in the feedforward loop, which is designed to adjust the output thrusts to be the values mentioned before. Figure 2 shows the response of the system under these two structures, where one of the engines (dashed curve) becomes unhealthy at 300 s. From that point onwards, the healthy engine (solid curve) carries more responsibility in terms of thrust load, and the total thrust produced by the engines (dotted curve) before and after the distribution of the load is equal. It is concluded that both feedback control in Fig. 2(a) and feedforward control in Fig. 2(b) effectively serve the purpose of load distribution without violating the constraint of total thrust output.

Although the load is redistributed among the engines, another effect of this action is to introduce an excess moment along the yaw axis of the aircraft. Therefore, it is the responsibility of the flight control system to take care of this yaw moment. The details of this subject will be discussed later.
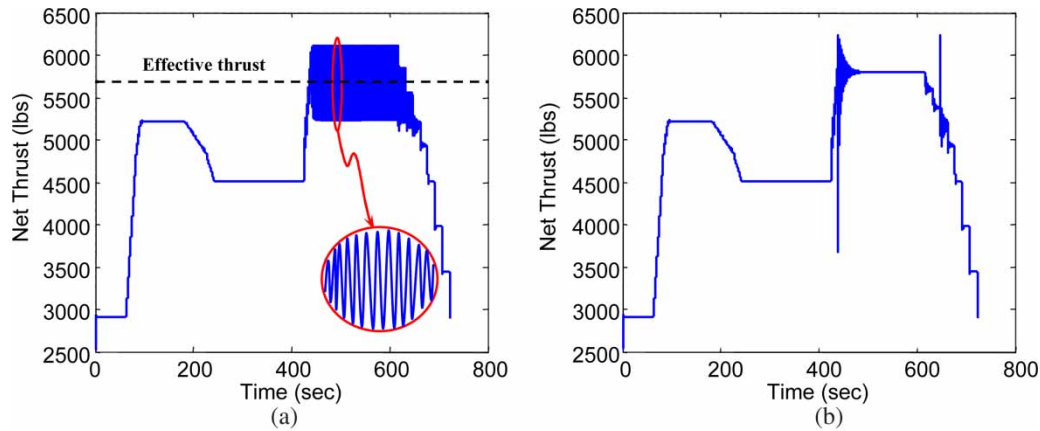
Fig. 1 Thrust output of the engine with and without supervisory action (a) without supervisory action (b) with supervisory action

3 AIRCRAFT MODEL AND INTEGRATION

This section discusses a generic model of full-envelope non-linear flight dynamics including the aerodynamic (control) surfaces. The operational envelope of the aircraft for trimmed, straight-and-level, 1 g flight is provided by Brumbaugh [26]. However, the actual model is tested for the full flight envelope to determine the real trim conditions and trust requirements to maintain these conditions. Figure 3 shows the flight envelope with solid curve and actual trimmed points of the model in Fig. 3(a) together with the net thrust output of the engines at these trimmed points in Fig. 3(b).
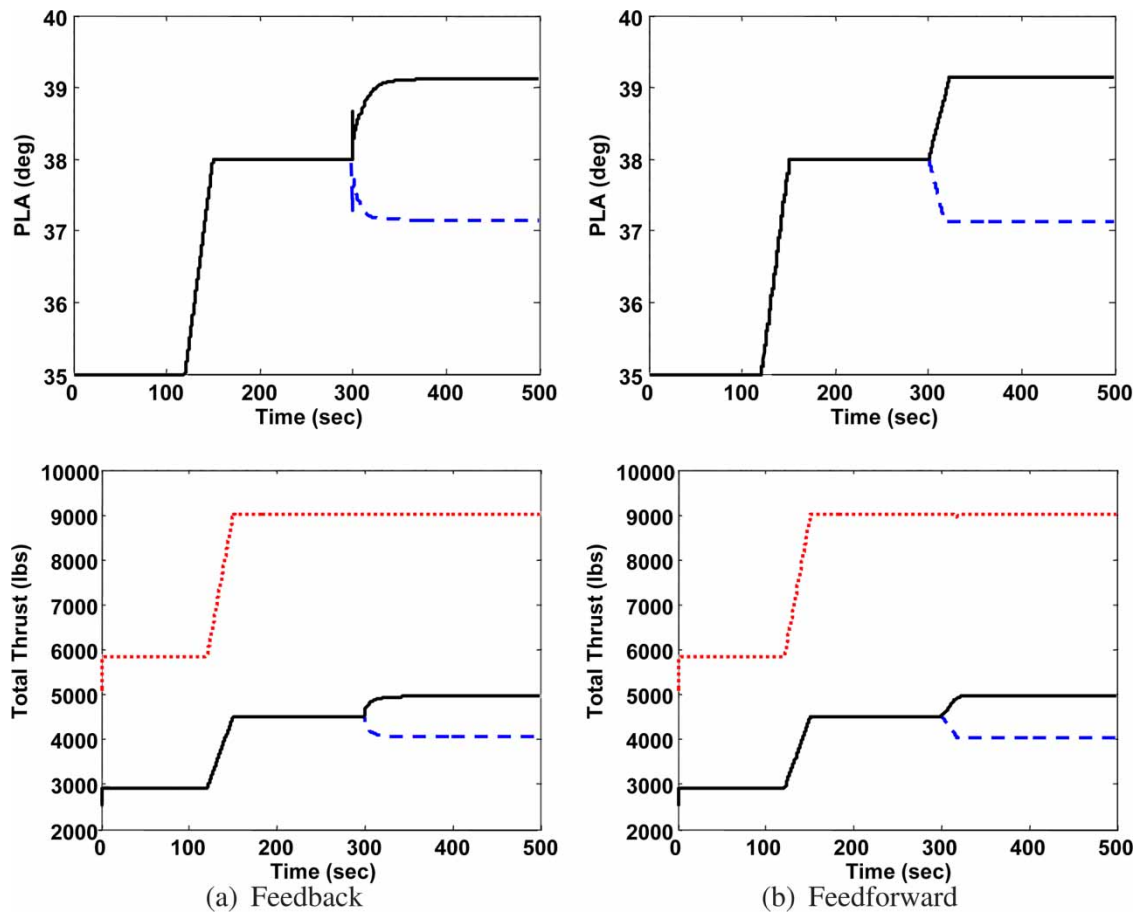
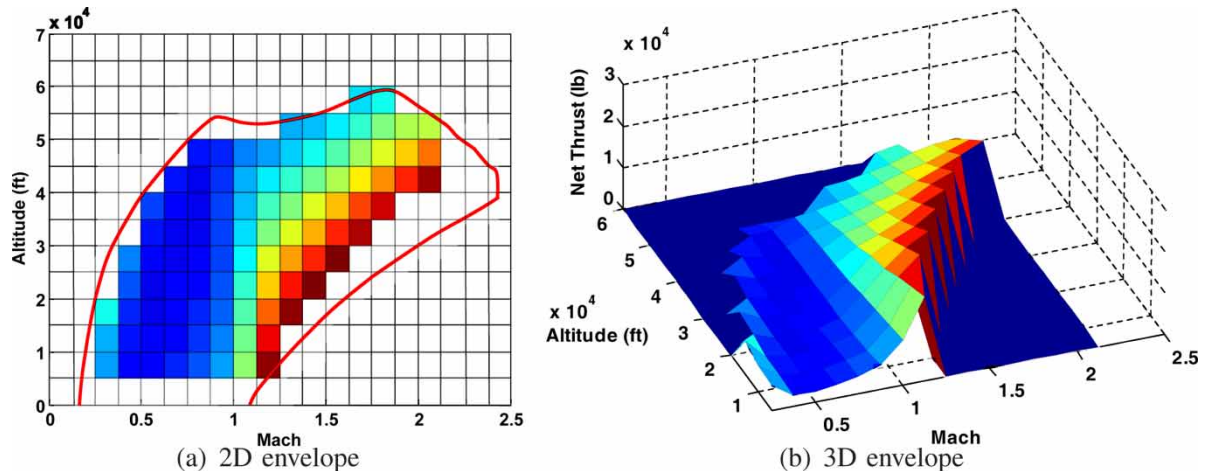**Fig. 2** Thrust distribution response of engines

Fig. 3 Provided and the actual operational envelopes of the aircraft

Integration of the flight dynamic model with the engine model is briefly described. This integrated flight-propulsion model represents a high performance supersonic aircraft, which is powered by two afterburning turbofan engines [**26**]. The primary control surfaces of the aircraft consist of right and left ailerons, two horizontal elevators (stabilator), and a single vertical rudder, where elevators are capable of symmetric and differential motion. All the five actuators in the model corresponding to each control surface have identical first-order response given by

$$G(s) = \frac{20}{s + 20}$$

The actuator commands are not easily predictable because of the non-linear interactions in the command paths.

The equations defining the aerodynamic model provide non-dimensional force and moment coefficients, which are functions of Mach number (**M**), angle of attack (α), and angle of sideslip (β). The non-linear equations of motion, used in the model, are general six-degree-of-freedom equations representing the flight dynamics of a rigid aircraft flying in a stationary atmosphere over a flat, non-rotating earth. There are 13 state variables in the model for which the details of the derivation of state equations can be found in reference [**27**]. Pertinent governing equations of flight dynamics are given in Appendix 3.

The linear gain-scheduled control law of the aircraft is synthesized based on the linearized models of the plant dynamics, which are obtained at various points of flight operation. An equally spaced grid of 36 points of operation is chosen in order to derive the linearized models of the flight dynamics including the stability derivatives and trim states as well as the trim values of the controls. Integration of the flight and engine models necessitates the replacement of the propulsion model embedded in the flight dynamics with the DES-controlled propulsion system in hand.

The aircraft under consideration consists of two engines, where each engine thrust vector is aligned with the body axis and acts at a point located ∼3m behind the center of gravity of the vehicle and ∼1.2 m laterally from the centre-line. The thrust produced by each engine is a function of altitude, Mach number, and throttle setting and is observed to have a maximum value of ∼10 900 kgf. Throttle position inputs to the engines are in degrees between the minimum of 20° and the maximum of 127°. The afterburner section begins to respond at a throttle position of 91° [**26**].

The generic model of the turbofan engine performs between throttle settings (or PLA) of 21°–50°, and the afterburner section of the model responds after 42.5°. The engine model can produce thrust output of 12 600 lbf (∼5730 kgf) at the maximum throttle setting. Therefore, it is mandatory to closely match the input–output relationships of the aircraft engine model and the generic engine model; this issue is addressed by integration of the aircraft and engine models as seen in Fig. 4. However, as there is more than one option to use the engine model as an integral part of the aircraft model, it is essential to decide on the functions $f_1(\bullet)$ and $f_2(\bullet)$, which map the PLAs, $\text{PLA}^{\text{Flight}}(\text{PLA}^{\text{F}})$ to $\text{PLA}^{\text{Engine}}(\text{PLA}^{\text{E}})$, and thrusts, $F_N^{\text{Engine}}(F_{\text{E}}^N)$ to $F_N^{\text{Flight}}(F_{\text{F}}^N)$, respectively. One of the ways to obtain these mappings is first to decide on the function $f_1(\bullet)$, and then match up the three-dimensional thrust profiles of the models using the function $f_2(\bullet)$.

The affine function $f_1(x) = ax + b$ is a commonly used method of mapping PLA^{F} to PLA^{E} if the desired limits on the maximum and minimum values of the throttle settings can be attained in this way. The affine mapping has been adopted in this paper to convert all recorded PLA^{F} values to achieve the necessary thrust requirements that are provided in Fig. 3(b).
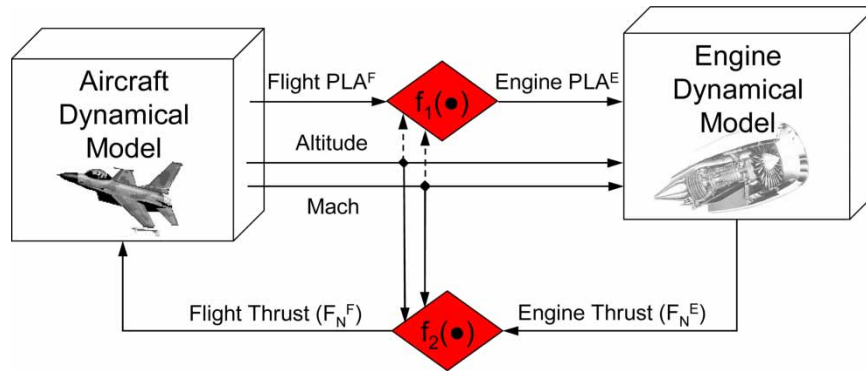
Fig. 4   Integration of aircraft and engine models while preserving the input–output relationships

Net thrust output of the engine model for the whole flight envelope of the aircraft is given in Fig. 5(b). As it is seen in Fig. 5(a), the engine model cannot be trimmed at some of the operating points of the flight model. These points should be avoided during the integrated flight. A comparison of Fig. 3 with Fig. 5 reveals that the function $f_2(\bullet)$, mapping F_N^E to F_N^F, is not easy to obtain, although point-by-point ratio of $K = F_N^F/F_N^E$ is readily available. Therefore, it is useful to describe the relation between PLA^E and ratio K.

Figure 6 is a good representative of the engine systems in terms of thrust output and PLA input. Owing to the controller dynamics embedded in the engine model, the response of the engine remains linear with respect to PLA input even if the afterburner starts to take action. In the aircraft model, however, the afterburner response of the engine is non-linear, the effects of afterburner response can easily be observed around 42.5° of throttle position where the response of the models start to separate from each other considerably. As a result of the separation between models at the point where afterburner effects are observable,

the curve fitting to the K versus PLA relation needs a piecewise linear or an exponential form if more information is preserved. However, this method for the integration of the models involves additional non-linear dynamics to the response of the overall system. This can be circumvented by using a linear fit to the data points of the relation K versus PLA with the penalty of increasing scaling errors, especially for high PLA values.

4   PARAMETER-SCHEDULING DYNAMIC-INVERSION CONTROL LAW

This section elaborates the control law that is used to manoeuvre the aircraft under different engine loading conditions. The parameter-scheduling type dynamic-inversion control law effectively stabilizes the aircraft in full operating envelope. The linear model inverting control concept is often used in non-linear aircraft control applications along with some adaptation rule [20, 28].
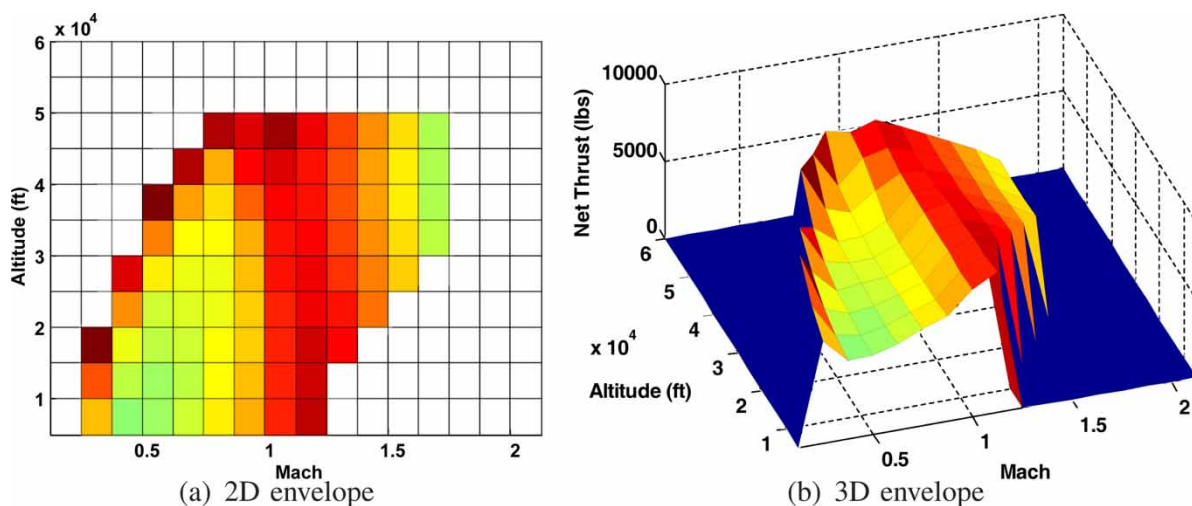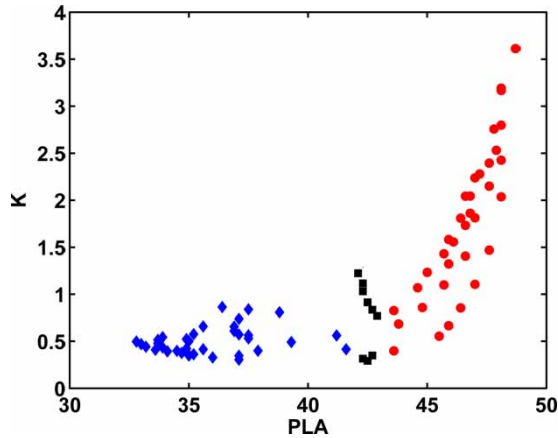

Fig. 5   Engine thrust outputs obtained in the aircraft flight envelope

Fig. 6 Thrust ratio relation as a function of throttle position

The short-period longitudinal dynamics of an aircraft can be approximated by the linear system

$$\begin{bmatrix} \Delta\dot{\alpha} \\ \dot{q} \end{bmatrix} = \begin{bmatrix} Z_\alpha & 1 \\ M_\alpha & M_q \end{bmatrix} \begin{bmatrix} \Delta\alpha \\ q \end{bmatrix} + \begin{bmatrix} Z_{\delta_e} \\ M_{\delta_e} \end{bmatrix} \Delta\delta_e + \begin{bmatrix} Z_{\delta_t} \\ M_{\delta_t} \end{bmatrix} \Delta\delta_t$$

where the stability and control derivatives ($Z_\alpha, Z_{\delta_e}, Z_{\delta_t}, M_\alpha, M_q, M_{\delta_e}$, and M_{δ_t}) and the trim state and control variables (α_0, δ_{e0}, are δ_{t0}) are functions of the altitude, h, and Mach number, $\mathbf{M}$ (see also the Appendix 1). In the linearized models, the states and controls are represented as perturbations from the trim condition as $\Delta\alpha \triangleq \alpha - \alpha_0$, $\Delta\delta_e \triangleq \delta_e - \delta_{e0}$, and $\Delta\delta_t \triangleq \delta_t - \delta_{t0}$

The above system of first-order equations can be transformed to a single second-order equation (by dropping the control rate terms)

$$\Delta\ddot{\alpha} = \left(Z_\alpha^2 + M_\alpha\right)\Delta\alpha + (Z_\alpha + M_q)q \\ + (Z_\alpha Z_{\delta_e} + M_{\delta_e})\Delta\delta_e + (Z_\alpha Z_{\delta_t} + M_{\delta_t})\Delta\delta_t$$

If the following control law for the elevator deflection is used

$$\Delta\delta_e = \frac{\begin{aligned}v_\alpha - (Z_\alpha^2 + M_\alpha)\Delta\alpha - (Z_\alpha + M_q)\\ \times q - (Z_\alpha Z_{\delta_t} + M_{\delta_t})\Delta\delta_t\end{aligned}}{Z_\alpha Z_{\delta_e} + M_{\delta_e}}$$

then the pitch dynamics are reduced to $\Delta\ddot{\alpha} = v_\alpha$, where v_α is called the pseudo-control and represents the desired angle of attack acceleration. The pseudo-control can be defined to follow an ideal response to pilot commands using a command filter. In addition, it can include feedback terms in order to reject disturbances with desired error dynamics.

The method described above is shown for a linear system. However, in practice, the method can be applied to non-linear aircraft dynamics with reasonable accuracy using either an adaptive scheme [**28**] or by scheduling the stability derivatives, trim states, and

controls with flight condition. In this case, a scheduling approach is used where the flight condition is represented by the altitude, h, and Mach number, $\mathbf{M}$.

The desired angle of attack is given by the command filter

$$\begin{bmatrix} \dot{\alpha}_d \\ \ddot{\alpha}_d \end{bmatrix} = \begin{bmatrix} 0 & 1 \\ -\omega_n^2 & 2\xi\omega_n \end{bmatrix} \begin{bmatrix} \alpha_d \\ \dot{\alpha}_d \end{bmatrix} + \begin{bmatrix} 0 \\ \omega_n^2 \end{bmatrix} \alpha_{cmd}$$

The command filter is used to calculate the desired values of angle of attack and its first and second derivative ($\alpha_d, \dot{\alpha}_d$, and $\ddot{\alpha}_d$) in order to achieve the desired second-order response to the angle of attack commands from the pilot (α_{cmd}). The pseudo-control is then calculated using the following control law

$$v_\alpha = \ddot{\alpha}_d + K_P(\alpha_d - \alpha) + K_D(\dot{\alpha}_d - \dot{\alpha})$$

Defining the tracking error as $\tilde{\alpha} = \alpha_d - \alpha$, the error dynamics are governed by

$$\ddot{\tilde{\alpha}} + K_D\dot{\tilde{\alpha}} + K_P\tilde{\alpha} = 0$$

The proportional and derivative gains, K_P and K_D, can be selected to ensure stable second-order error dynamics. A reasonable method of selecting the gains is such that the error dynamics have the same natural frequency and damping as the command filter $K_P = \omega_n^2$ $K_D = 2\xi\omega_n$. In this way, the dynamic response to a disturbance will be similar to pilot commands.

The lateral directional controller is designed using a similar method as described previously for longitudinal dynamics of an aircraft except the fact that the dynamic inversion of the model is required. The dynamics care represented by

$$\begin{bmatrix} \dot{p} \\ \dot{\beta} \\ \dot{r} \end{bmatrix} = \begin{bmatrix} L_p & L_\beta & L_r \\ Y_p + \tan\alpha & Y_\beta & Y_r - 1 \\ N_p & N_\beta & N_r \end{bmatrix} \begin{bmatrix} p \\ \beta \\ r \end{bmatrix} \\ + \begin{bmatrix} L_{\delta_a} & L_{\delta_r} \\ Y_{\delta_a} & Y_{\delta_r} \\ N_{\delta_a} & N_{\delta_r} \end{bmatrix} \begin{bmatrix} \delta_a \\ \delta_r \end{bmatrix} + \begin{bmatrix} L_{\delta_{dt}} \\ Y_{\delta_{dt}} \\ N_{\delta_{dt}} \end{bmatrix} \delta_{dt} \\ + \begin{bmatrix} 0 \\ \dfrac{g}{V}\cos\theta\sin\phi \\ 0 \end{bmatrix}$$

Note that the last term, δ_{dt}, represents differential thrust. It is important to account for this term so that the controller performs well when the engine load balancing changes.

The objective of the lateral-directional controller is to track commands for sideslip angle, β, and stability axis roll rate, $p_s = p\cos\alpha + r\sin\alpha$. As with the longitudinal controller, the last two equations are converted to a single second-order equation in β. The linearized
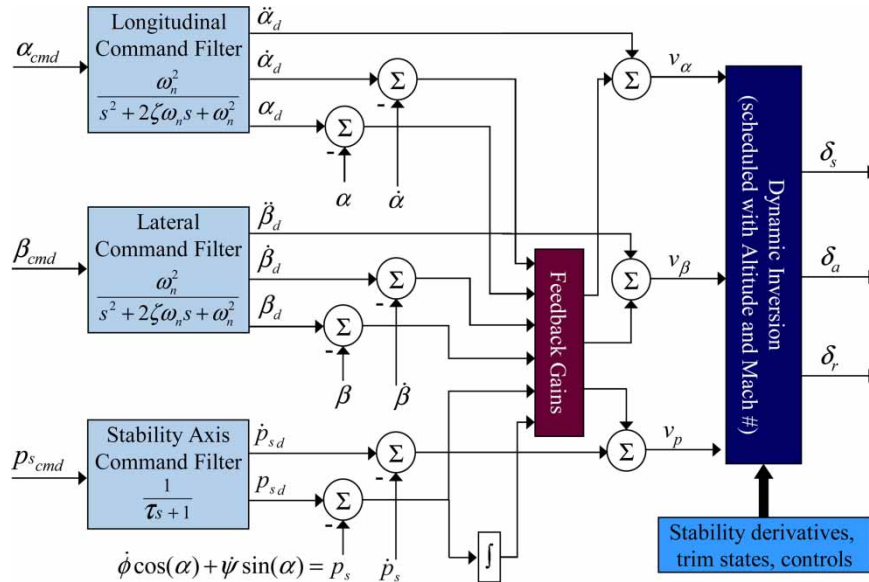
Fig. 7 Scheme of the flight control law

model is parameterized by angle of attack to account for stability axis roll

$$\begin{bmatrix} \dot{p}_s \\ \ddot{\beta} \end{bmatrix} = \mathbf{A} \begin{bmatrix} p \\ \beta \\ r \end{bmatrix} + \mathbf{B_1} \begin{bmatrix} \delta_a \\ \delta_r \end{bmatrix} + \mathbf{B_2}\delta_{dt} + \mathbf{g}$$

where

$$\mathbf{A} = \left[\begin{array}{c} L_p \cos \alpha + N_p \sin \alpha \\ Y_\beta Y_p + (Y_p + \tan \alpha)L_p + (Y_r - 1)N_p \end{array} \right.$$

$$L_\beta \cos \alpha + N_\beta \sin \alpha$$
$$Y_\beta^2 + (Y_p + \tan \alpha)L_\beta + (Y_r - 1)N_\beta$$

$$\left. \begin{array}{c} L_r \cos \alpha + N_r \sin \alpha \\ Y_\beta Y_r + (Y_p + \tan \alpha)L_r + (Y_r - 1)N_r \end{array} \right]$$

$$\mathbf{B_1} = \left[\begin{array}{c} L_{\delta_a} \cos \alpha + N_{\delta_a} \sin \alpha \\ Y_\beta Y_{\delta_a} + (Y_p + \tan \alpha)L_{\delta_a} + (Y_r - 1)N_{\delta_a} \end{array} \right.$$

$$\left. \begin{array}{c} L_{\delta_r} \cos \alpha + N_{\delta_r} \sin \alpha \\ Y_\beta Y_{\delta_r} + (Y_p + \tan \alpha)L_{\delta_r} + (Y_r - 1)N_{\delta_r} \end{array} \right]$$

$$\mathbf{B_2} = \left[\begin{array}{c} L_{\delta_{dt}} \cos \alpha + N_{\delta_{dt}} \sin \alpha \\ Y_\beta Y_{\delta_{dt}} + (Y_p + \tan \alpha)L_{\delta_{dt}} + (Y_r - 1)N_{\delta_{dt}} \end{array} \right]$$

$$\mathbf{g} = \left[\begin{array}{c} 0 \\ \frac{g}{V}(Y_\beta \cos \theta \sin \phi + \cos \theta \cos \phi \dot{\phi} - \sin \theta \sin \phi \dot{\theta}) \end{array} \right]$$

The inversion control law is then given by

$$\begin{bmatrix} \delta_a \\ \delta_r \end{bmatrix} = \mathbf{B_1}^{-1} \left(\begin{bmatrix} v_p \\ v_\beta \end{bmatrix} - \mathbf{A} \begin{bmatrix} p \\ \beta \\ r \end{bmatrix} - \mathbf{B_2}\delta_{dt} - \mathbf{g} \right)$$

The yaw axis controller is designed to achieve a second-order sideslip response using a second-order command filter and proportional derivative controller similar to that used for angle of attack. The desired stability axis roll rate response is first order. Therefore, a first-order command filter is selected and a proportional plus integral compensator is used

$$v_\beta = \ddot{\beta}_d + K_P(\beta_d - \beta) + K_D(\dot{\beta}_d - \dot{\beta})$$

$$v_p = \dot{p}_{s_d} + K_P(p_{s_d} - p_s) + K_I \int (p_{s_d} - p_s)\,dt$$

The overall scheme of the parameter-scheduled dynamic-inversion control law for the flight dynamics is given in Fig. 7.

5 RESULTS OF THE INTEGRATED SYSTEM SIMULATION

The experimentation set-up for the integrated flight system is designed on the simulation test bed to validate the operation of DES-controlled propulsion system with other modules of the aircraft. Upon successful implementation of the software modules, several sets of experiments were conducted.

Loads of the two engines are redistributed when health condition of one engine is degraded [25] and the other engine functions normally. Owing to this imbalance of the generated thrust, the response of the aircraft to the aerodynamic forces may change drastically. As a typical case, Figs 8 and 9 show the changes in the attitude of the nominal closed-loop dynamical behaviour of the aircraft when DES controller decides to change the load distribution due to health conditions of the engines. In Fig. 8, thrust produced by individual engines is depicted (solid curve for healthy engine and dashed curve for unhealthy
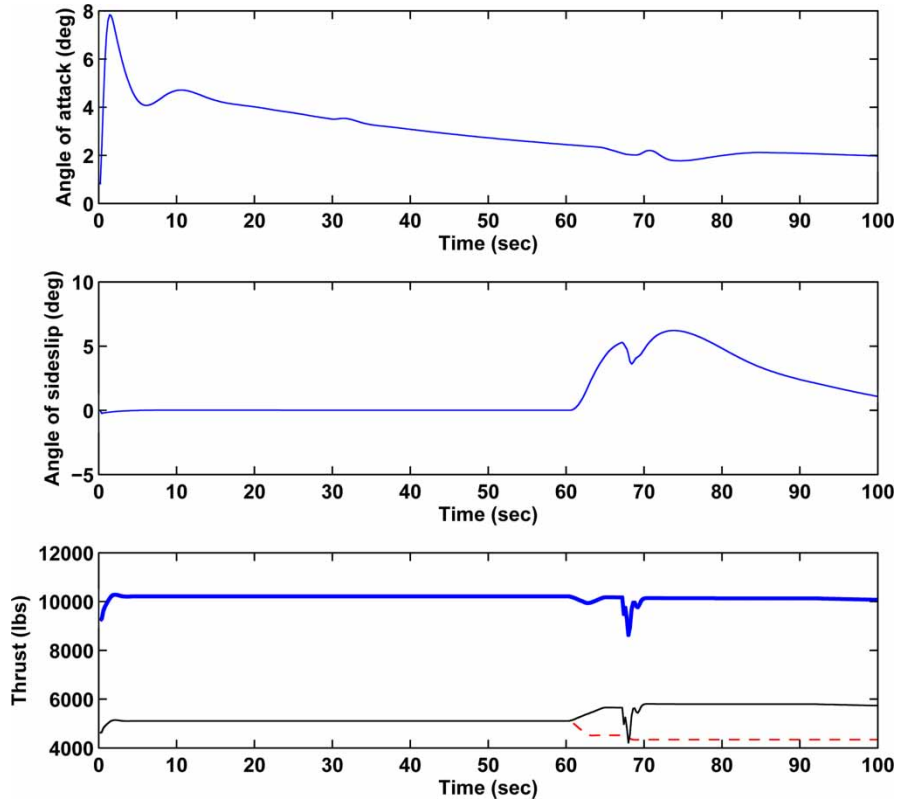
Fig. 8 Response of the aircraft to load distribution
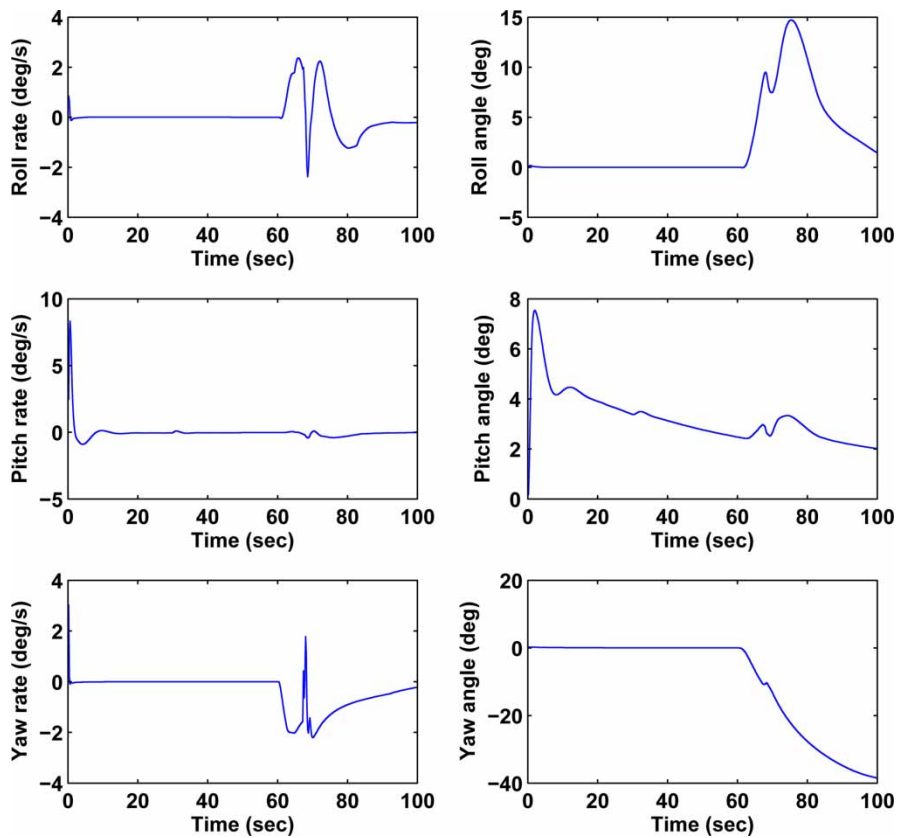

Fig. 9 Changes in the attitude of the aircraft after load distribution
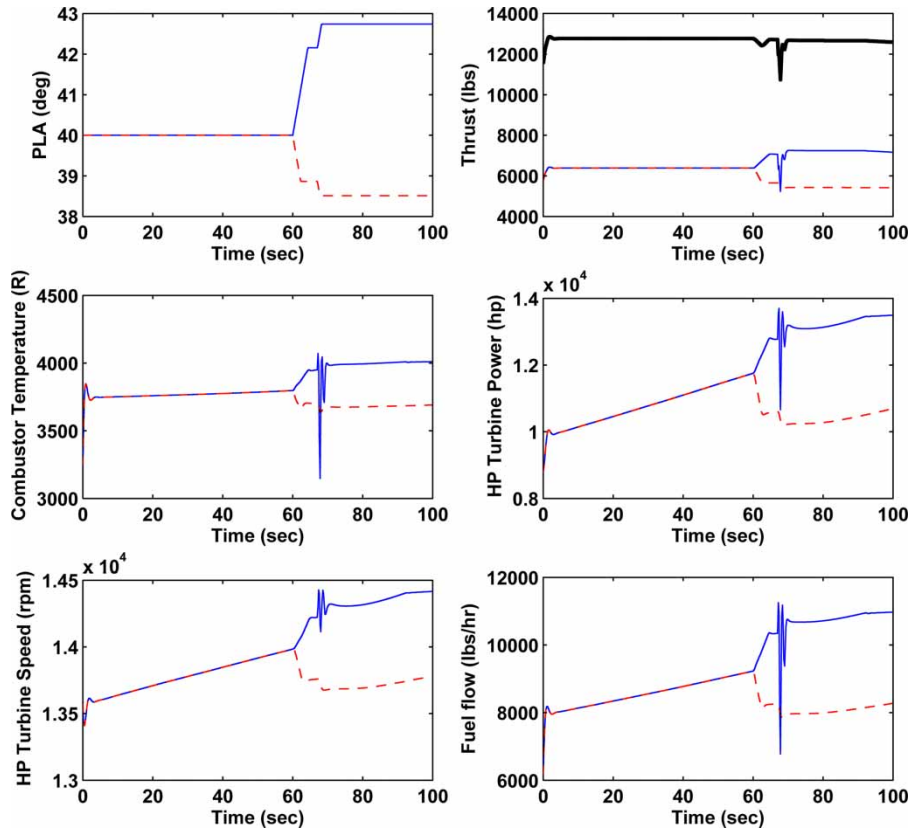
Fig. 10   Response of the engines under dynamic flight conditions
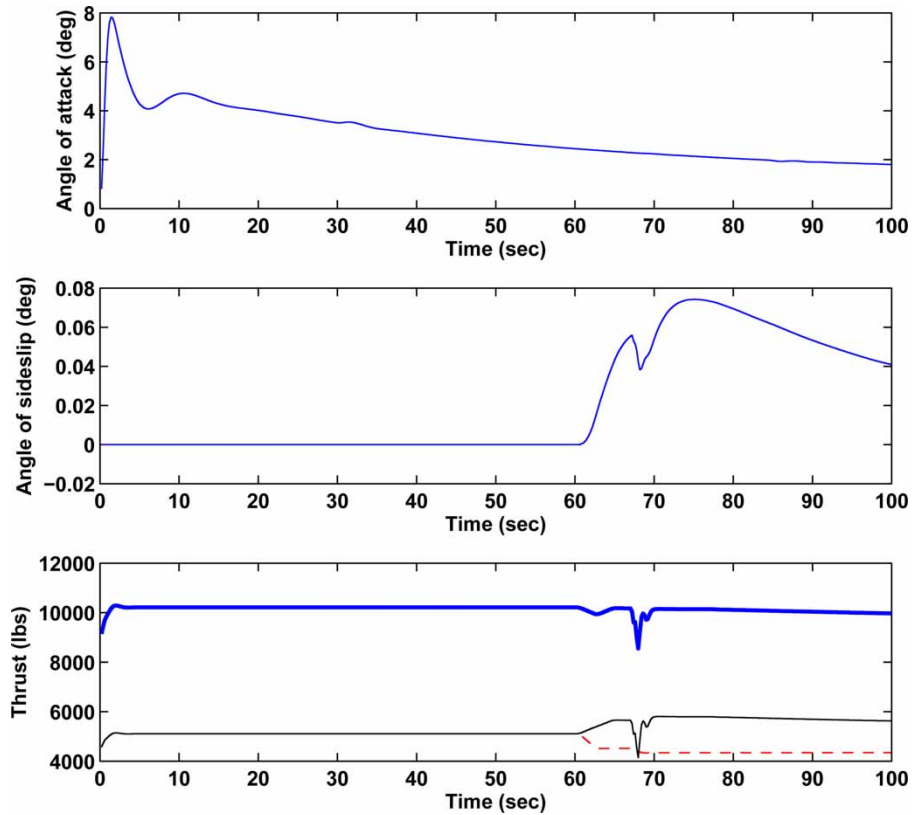

Fig. 11   Response of the aircraft to load distribution under dynamic-inversion control
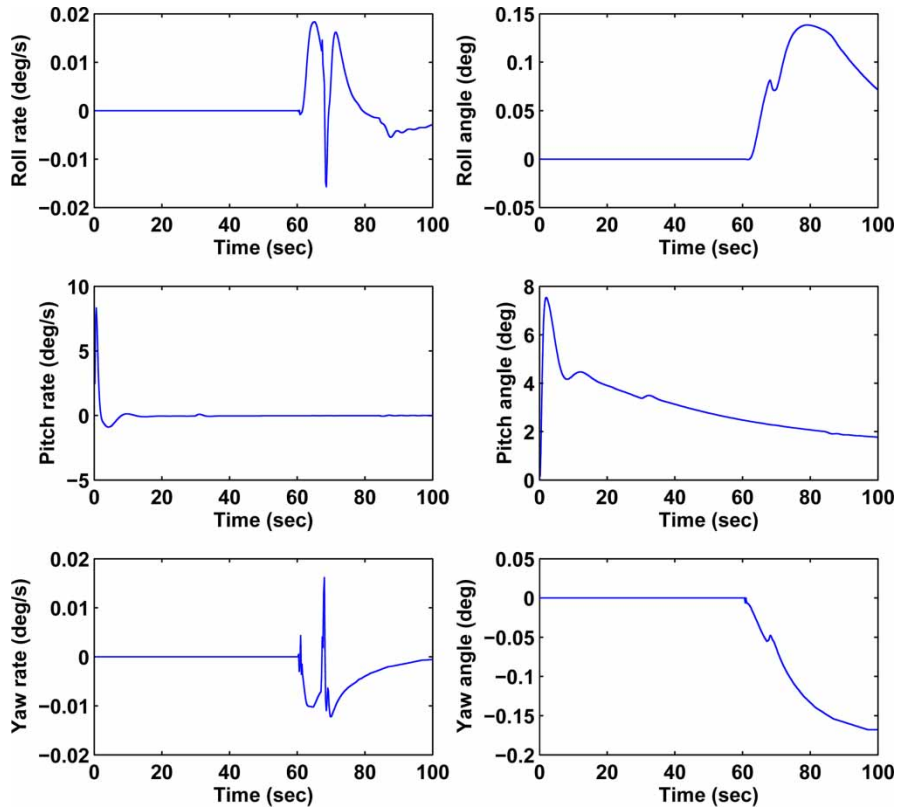
Fig. 12 Changes in the attitude of the aircraft under dynamic-inversion control
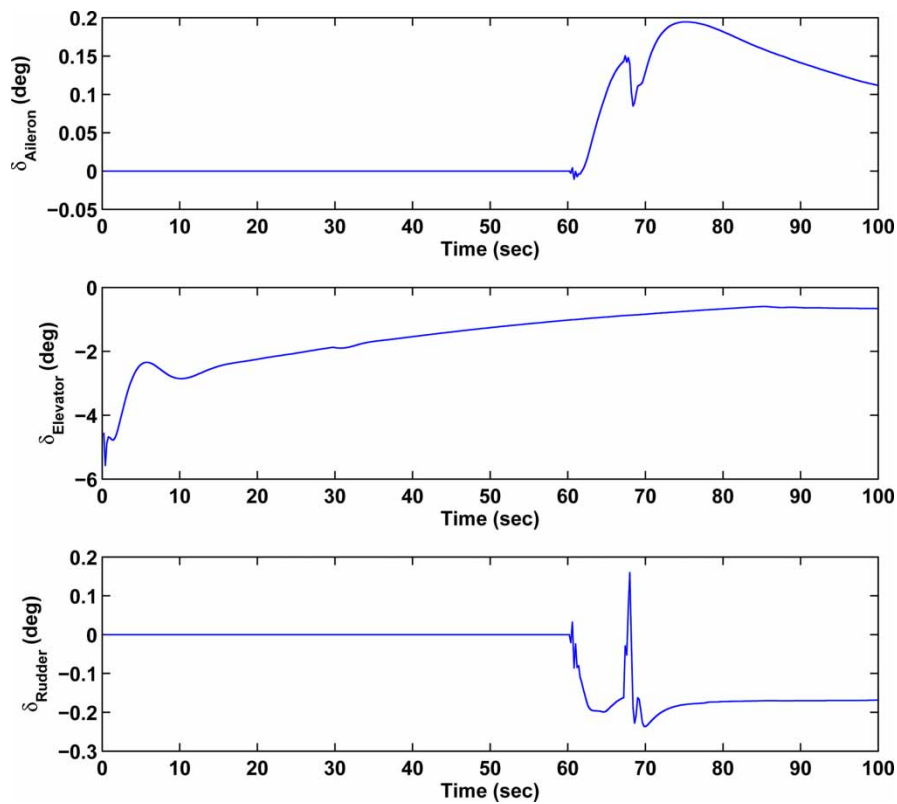

Fig. 13 Aileron, differential elevator, and rudder deflections

engine) as well as the total thrust (thick curve), and it is seen that load distribution is successfully accomplished in integrated system. It is also observed that the nominal controller successfully stabilizes the plant dynamics as both angle of attack (α) and angle of sideslip (β) reach steady-state values. However, the nominal flight control design for the aircraft does not account for the differential thrust. Therefore, in Fig. 9, the flight orientation angles are adversely affected from load distribution; and the situation manifests in both roll and yaw angles as a departing behaviour from the nominal condition immediately after the thrust redistribution. As a result, the yaw angle settles to a steady-state value of $-38°$, which leads to divergence from nominal path of the aircraft.

Response of the engines in the same flight is presented in Fig. 10, and the solid curve represents the healthy engine and the dashed curve represents the response of the unhealthy engine. Thick curve in the upper right plate of Fig. 10 shows the total thrust output of the engines, which is kept unaltered before and after the load redistribution. This shows that DES control logic of the propulsion system, which incorporates the detection of engine degradation and the assessment of relative health status of engines, issues the load distribution command and works effectively under dynamic flight conditions. It is also important to note that afterburner of the engine steps in after PLA of $42.5°$ is applied, which results in discontinuous behaviour of the response for both engine and aircraft dynamics. It should also be noted that the thrust produced by the engines is scaled before going through the aircraft model.

Subsequently, the effects of load redistribution on the aircraft control surfaces under the dynamic-inversion controller with differential thrust accommodation is observed. The controller manipulates the control surfaces (ailerons, elevators and rudder) for regulating the roll angle and sideslip. Under this controller action, Figs 11 and 12 show the changes in the attitude of the closed-loop dynamical behaviour of the aircraft when DES controller decides to change the load distribution due to health conditions of the engines. It is seen that roll angle and yaw angle respond to load distribution much better than the nominal control case which indicates that flight control with differential thrust accommodation can handle the effects of DES decision reasonably. However, the controller still may cause a possible divergence from the desired path in the long term because the dynamic-inversion law is capable of controlling the yaw angle with a steady-state error of $-0.17°$. The rationale is that the dynamic-inversion control variable is the sideslip angle β instead of yaw angle ψ, and the control law does not contain a heading control *per se*. A possible and easily implementable solution could be introducing an outer feedforward bias to apply a corrective heading action, as the steady-state error of the yaw motion is constant.

Figure 13 depicts the deflection of the control surfaces due to control commands to overcome the effects of load imbalance and resulting moments created on the aircraft. Small deflections, which are much less than the provided limits [**26**], result in superior controlled behaviour of the aircraft in terms of roll and yaw angles.

6   SUMMARY, CONCLUSIONS AND FUTURE WORK

This paper presents a comprehensive control concept, from operational management to continuous-time regulation, for integrated flight/propulsion in advanced aircraft. The dynamic effects of DES control system on aircraft responses have been observed and adverse affects of DES decisions have been compensated with a dynamic-inversion control law. The control laws have been validated on a networked simulation test bed that incorporates coupled effects of both flight and propulsion dynamics. Future research pertaining to long-term objectives of the work reported in this paper are to develop:

(a) enhancement of aircraft autopilot and autonomous flight strategies for intelligent decision and control;
(b) decision-making and mission planning through a high-level DES coordinator under dynamic flight conditions;
(c) autonomous air and ground vehicles integration for decision-making and intelligent control of fleet operations in C^4ISR systems.

REFERENCES

1 **Ramadge, P. J.** and **Wonham, W. M.** Supervisory control of a class of discrete event processes. *SIAM J Control Optim.*, 1987, **25**(1), 206–230.
2 **Cassandras, C. G.** and **Lafortune, S.** *Introduction to discrete event systems*, 1999 (Kluwer Academic, Boston, MA, USA).
3 **Hopcroft, J. E., Motwani, R.,** and **Ullman, J. D.** *Introduction to automata theory, languages, and computation*, 2nd edition, 2001 (Addison-Wesley, Boston, MA, USA).
4 **Ray, A.** Signed real measure of regular languages for discrete event supervisory control. *Int. J. Control*, 2005, **78**(12), 949–967.

5 **Chattopadhyay, I.** and **Ray, A.** Renormalized measure of regular languages. *Int. J. Control*, 2006, **79**(9), 1107–1117.

6 **Chattopadhyay, I.** and **Ray, A.** Language-measure-theoretic optimal control of probabilistic finite state systems. *Int. J. Control*, 2007, **80**(8), 1271–1290.

7 **Tolani, D., Horn, J.,** and **Ray, A.** Integrated decision and control of human-engineered complex systems. *Int. J. Gen. Syst.*, 2006, **35**(3), 275–294.

8 **Tolani, D., Horn, J., Yasar, M.,** and **Ray, A.** Hierarchical control of rotorcraft for enhanced performance and structural durability. In the AIAA Guidance, Navigation, and Control Conference and Exhibit, San Francisco, CA, USA, 2005.

9 **Yasar, M.** and **Ray, A.** Hierarchical control of aircraft propulsion systems: discrete event supervisor approach. *Control Eng. Pract.*, 2007, **15**(2), 149–162.

10 **Kreiner, A.** and **Lietzau, K.** *The use of onboard real-time models for jet engine control*, 2003 (MTU Aero Engines, Munich, Germany).

11 **Ray, A.** and **Caplin, J.** Life extending control of aircraft: trade-off between flight performance and structural durability. *Aeronaut. J.*, 2000, **104**(1039), 397–408.

12 **Caplin, J., Ray, A.,** and **Joshi, S. M.** Damage-mitigating control of aircraft for enhanced structural stability. *IEEE Trans. Aerosp. Electron. Syst.*, 2001, **37**(3), 849–862.

13 **Garg, S., Mattern, D. L.,** and **Bullard, R. E.** Integrated flight/propulsion control system design based on a centralized approach. *AIAA J. Guid. Control Dyn.*, 1991, **14**(1), 107–116.

14 **Menon, P. K., Iragavarapu, V. R.,** and **Garg, S.** Enhancing aircraft performance through flight/propulsion system integration. In the AIAA Guidance, Navigation and Control Conference, San Diego, CA, 1996.

15 **McWilliams, L. H., Raven, E. A.,** and **Sain, P. M.** A study of a propulsion control system for a VATOL aircraft. In Proceedings of the IEEE National Aerospace and Electronics Conference, Dayton, Ohio, USA, 1989, vol. 1, pp. 356–363.

16 **Bates, D. G., Gatley, S. L.,** and **Postlethwaite, I.** Integrated flight and propulsion control system design using H1 loop-shaping techniques. In Proceedings of the Conference on Decision and Control, Phoenix, AZ, 1999, pp. 1523–1528.

17 **Garg, S.** Partitioning of centralized integrated flight/propulsion control design for decentralized implementation. *IEEE Trans. Control Systems Technol.*, 1993, **1**(2), 93–100.

18 **Harefors, M.** and **Bates, D. G.** Integrated propulsion-based flight control system for a civil transport aircraft. In Proceedings of the IEEE International Conference on Control Applications, Glasgow, UK, 2002, pp. 132–137.

19 **Schmidt, P. H., Garg, S.,** and **Holowecky, B. R.** A parameter optimization approach to controller partitioning for integrated flight/propulsion control application. *IEEE Trans. Control Systems Technol.*, 1993, **1**(1), 21–36.

20 **Rysdyk, R.** and **Calise, A. J.** Robust nonlinear adaptive flight control for consistent handling qualities. *IEEE Trans. Control Systems Technol.*, 2005, **13**(6), 896–910.

21 **Diao, Y.** and **Passino, K. M.** Stable fault-tolerant adaptive fuzzy/neural control for a turbine engine. *IEEE Trans. Control Systems Technol.*, 2001, **9**(3), 494–509.

22 **Parker, K. I.** and **Guo, T. H.** Development of a turbofan engine simulation in a graphical simulation environment. In JANNAF Aero-Propulsion Subcommittee Meeting, Destin, FL, USA, 2002.

23 **Adibhatla, S.** and **Johnson, K. L.** Evaluation of nonlinear PSC algorithm on a variable cycle engine. In the AIAA Joint Propulsion Conference and Exhibit, Monterey, CA, 1993.

24 **Perry, A. R.** The flightgear flight simulator. In the USENIX Annual Technical Conference, Boston, MA, USA, 2004.

25 **Tolani, D., Yasar, M., Ray, A.,** and **Yang, V.** Anomaly detection in aircraft gas turbine engines. *J. Aerosp. Comput. Inf. Commun.*, 2006, **3**(2), 44–51.

26 **Brumbaugh, R. W.** An aircraft model for the AIAA controls design challenge. *J. Guid. Control Dyn.*, 1994, **17**(4), 747–752.

27 **Duke, E. L., Antoniewicz, R. F.,** and **Krambeer, K. D.** Derivation and definition of a linear aircraft model. NASA Dryden Flight Research Center, Edwards, CA, USA, RP-1207, 1998.

28 **Calise, A., Lee, S.,** and **Sharma, M.** Development of a reconfigurable flight control law for the X-36 tailless fighter aircraft. In the AIAA Guidance, Navigation and Control Conference, Denver, CO, USA, 2000.

APPENDIX 1

Notation

g	acceleration due to gravity (ft/s^2)
h	altitude (ft)
K_D	differential control gain
K_I	integral control gain
K_P	proportional control gain
L	total body axis aerodynamic rolling moment (lb ft)
$\mathbf{M}$	Mach number
M	total body axis aerodynamic pitching moment (lb ft)
N	total body axis aerodynamic yawing moment (lb ft)
p	roll rate (rad/s)
p_s	stability axis roll rate (rad/s)
q	pitch rate (rad/s)
r	yaw rate (rad/s)
s	complex frequency
T_a	ambient temperature (K)
V	total velocity (ft/s)
Y	total side force along the y-body axis (lb)
Z	total force along the z-body axis (lb)
α	angle of attack (rad)
β	angle of side slip (rad)
δ_a	aileron deflection
δ_{dt}	differential thrust
δ_e	elevator deflection
δ_r	rudder deflection
δ_t	thrust command

θ	pitch angle (rad)
ν	pseudo-control
ξ	damping ratio of the command filter
ϕ	roll angle (rad)
ψ	heading angle (rad)
ω_n	natural frequency of the command filter

Subscripts

cmd	commanded value
d	desired value
0	steady-state value

APPENDIX 2

Pertinent governing equations of the engine model

This appendix succinctly derives the governing equations of the simulation model of a generic two-spool, low-bypass turbofan engine [22]. Performance maps have been used extensively in the simulator to provide steady-state representations of the engine's rotating components. Fluid momentum in the bypass duct and the augmentor, mass and energy storage within control volumes, and rotor inertias are also included to provide transient capability. For completeness of the paper, the pertinent model equations of the major components of the engine system are provided below in simplified forms.

Flight conditions and inlet

Gas turbine engines have an inlet for free stream air flowing into the engine. The following equations define the flight conditions and inlet model

$$P_\mathrm{amb} = f_1(a)$$
$$T_\mathrm{amb} = f_2(a)$$

where f_1 and f_2 are curve-fitted functions that are generated from atmospheric data. The equations for pressure, temperature, and enthalpy at the fan inlet are given by

$$P_2 = P_\mathrm{amb} \cdot \phi(M) \cdot \left[1.0 + \frac{(\gamma_1 - 1)M^2}{2}\right]^{\gamma_1/(\gamma_1 - 1)}$$
$$T_2 = T_\mathrm{amb}\left[1.0 + \frac{(\gamma_1 - 1)M^2}{2}\right]$$
$$h_2 = c_\mathrm{p}T_2$$

where

$$\phi = 1.0 \quad \text{if} \quad M \leqslant 1.0$$
$$\quad = 1.0 - 0.075(M - 1.0)^{1.35} \quad \text{if} \quad M > 1.0$$
$$\gamma_1 = 1.4$$

Fan

Fan performance is represented by a set of performance maps. Separate maps are used for the tip and hub sections of the fan. These maps are assumed to represent fan performance with variable geometry at nominal and scheduled positions. Map-generated, fan-corrected airflow is adjusted to account for off-schedule geometry effects. The following equations describe the fan model

$$P_{21} = P_2 \cdot f_3\left(\frac{P_2}{P_\mathrm{amb}}, \sqrt{\theta_2}, N_L\right)$$
$$h_{21} = h_2 + 5.858 \times 10^{-5} \, T_2 \cdot f_4(\psi_\mathrm{F}, \zeta_\mathrm{F})$$
$$T_{21} = f_5(h_{21})$$
$$\eta_\mathrm{F} = \frac{h_{21} - h_2}{h_{21}}$$
$$w_{21} = f_6\left(\sqrt{\theta_2}, \frac{P_{21}}{P_\mathrm{amb}}, N_L\right)$$
$$\mathrm{PW}_\mathrm{F} = (h_{21} - h_2) \cdot w_{21}$$
$$\mathrm{SM}_\mathrm{F} = \left(k_2 \cdot \frac{w_{21}}{P_{21}/P_\mathrm{amb}} - 1\right) \times 100$$

where f_3, f_4, f_5, and f_6 are the performance maps of the fan, which are provided in tabular formats in the engine simulation programme; and k_2 the fan stall line parameter due to distortion.

Booster and high-pressure compressor

Modern large turbofan engines usually have axial compressors. Performance maps are used for the compressor with a shift in the corrected airflow based on off-schedule values of variable-geometry position. The following equations describe the booster model and the high-pressure compressor model

$$h_{27\mathrm{d}} = 5.858 \times 10^{-5} \cdot f_7(\psi_\mathrm{B}, \zeta_\mathrm{B})$$
$$\eta_\mathrm{B} = \frac{h_{27\mathrm{d}} - h_{21}}{h_{27\mathrm{d}}}$$
$$w_{27\mathrm{d}} = f_8\left(\sqrt{\theta_{27\mathrm{d}}}, \frac{P_{27\mathrm{d}}}{P_\mathrm{amb}}, N_H\right)$$
$$\mathrm{PW}_\mathrm{B} = (h_{27\mathrm{d}} - h_{21}) \cdot w_{27\mathrm{d}}$$
$$\mathrm{SM}_\mathrm{B} = \left(k_{27\mathrm{d}} \cdot \frac{w_{27\mathrm{d}}}{(P_{27\mathrm{d}}/P_\mathrm{amb})} - 1\right) \times 100$$

where f_7 and f_8 are performance maps of the booster, which are provided in tabular formats in the engine simulation programme; and $k_{27\mathrm{d}}$ the booster stall line

parameter due to distortion

$$h_3 = 5.858 \times 10^{-5} \cdot f_9(\psi_{\mathrm{HPC}}, \zeta_{\mathrm{HPC}})$$

$$\mathrm{CPR} = \left(\frac{h_3}{0.239\,95} + 1 \right)^{\gamma_{21}/(\gamma_{21}-1)}$$

$$P_3 = P_{21} \cdot \mathrm{CPR}$$

$$\frac{T_3}{T_{21}} = \left(\frac{P_3}{P_{21}} \right)^{(\gamma_{21}-1)/\gamma_{21}}$$

$$\eta_{\mathrm{HPC}} = \frac{h_3 - h_{21}}{h_3}$$

$$w_3 = f_{10} \left(\sqrt{\theta_3}, \frac{P_3}{P_{\mathrm{amb}}}, N_H \right)$$

$$\mathrm{PW}_{\mathrm{HPC}} = (h_3 - h_{21}) \cdot w_3$$

$$\mathrm{W}_{\mathrm{HPC}} = \frac{c_p \cdot T_{21}}{\eta_3} \left[\mathrm{CPR}^{(\gamma_{21}-1)/\gamma_{21}} - 1 \right]$$

$$\mathrm{SM}_{\mathrm{HPC}} = \left(k_3 \cdot \frac{w_3}{(P_3/P_{\mathrm{amb}})} - 1 \right) \times 100$$

where f_9 and f_{10} are performance maps of the high-pressure compressor, which are provided in tabular formats in the engine simulation programme; and k_3 the compressor stall line parameter due to distortion.

Combustor

Total pressure losses are included in the models of main combustor, bypass duct, mixer entrance, and augmentor. Heat generation associated with the burning of fuel in the main combustor is assumed to take place at a constant combustor volume

$$P_4 = P_3 - 7.57 \times 10^{-4} w_3^2 \cdot \frac{T_3}{P_3}$$

$$h_4 = \frac{h_3 + (f/a)_4 \cdot \eta_{\mathrm{C}} \cdot Q}{\left[1 + (f/a)_4 \right]}$$

$$T_4 = \frac{h_4}{c_p}$$

The combustor health parameter (ψ_{C}) is a scaling factor for combustor efficiency η_{C}.

Power turbines

In the two-spool turbofan engine, high-pressure and low-pressure turbines produce engine thrust and also drive the compressor and the fan, respectively. Performance of the high- and low-pressure turbines is represented by performance maps. Cooling bleed for each turbine is assumed to re-enter the cycle at the turbine discharge, although a portion of each bleed is assumed to contributed to the power generated by the turbines

$$\mathrm{TPR}_{\mathrm{HPT}} = \frac{P_{45}}{P_4}$$

$$\frac{T_{45}}{T_4} = \left(\frac{P_{45}}{P_4} \right)^{(\gamma_4 - 1)/\gamma_4}$$

$$h_{45} = c_p T_{45}$$

$$\eta_{\mathrm{HPT}} = f_{11}(h_{45}, h_4, \psi_{\mathrm{HPT}})$$

$$w_{45} = f_{12} \left(N_H, \frac{\sqrt{T_{45}}}{P_4}, \zeta_{\mathrm{HPT}} \right)$$

$$W_{\mathrm{HPT}} = h_{45} - h_4 = c_p(T_{45} - T_4)$$

$$\mathrm{PW}_{\mathrm{HPT}} = (h_{45} - h_4) \cdot w_{45}$$

where f_{11} and f_{12} are performance maps of the high-pressure turbine, which are provided in tabular formats in the engine simulation programme

$$\mathrm{TPR}_{\mathrm{LPT}} = \frac{P_5}{P_{45}}$$

$$\frac{T_5}{T_{45}} = \left(\frac{P_5}{P_{45}} \right)^{(\gamma_{45}-1)/\gamma_{45}}$$

$$h_5 = c_p T_5$$

$$\eta_{\mathrm{LPT}} = f_{13}(h_5, h_{45}, \psi_{\mathrm{LPT}})$$

$$w_5 = f_{14} \left(N_L, \frac{\sqrt{T_5}}{P_{45}}, \zeta_{\mathrm{LPT}} \right)$$

$$W_{\mathrm{LPT}} = h_5 - h_{45} = c_p(T_5 - T_{45})$$

$$\mathrm{PW}_{\mathrm{LPT}} = (h_5 - h_{45}) \cdot w_5$$

where f_{13} and f_{14} are performance maps of the low-pressure turbine, which are provided in tabular formats in the engine simulation programme.

Nozzle

The nozzle is located downstream of the power turbines and does no work on the flow. A convergent–divergent nozzle configuration is assumed. The following equations describe the nozzle model

$$\mathrm{NPR} = \frac{P_8}{P_{\mathrm{amb}}}$$

$$\frac{T_8}{T_{\mathrm{amb}}} = \left(\frac{P_8}{P_{\mathrm{amb}}} \right)^{(\gamma_8 - 1)/\gamma_8}$$

$$h_8 = h_{8s} + \frac{V_8^2}{2\eta_8}$$

$$V_8 = \sqrt{2\eta_8 \cdot c_p T_8 \left[1 - \left(\frac{1}{\mathrm{NPR}} \right)^{(\gamma_8 - 1)/\gamma_8} \right]}$$

$$F_G = \frac{w_8(1.0244 - 0.6067 \cdot (f/a)_6)V_8}{32.17}$$

$$F_{ram} = w_2 \cdot M \cdot 1.5238\sqrt{T_{amb}}$$

$$F_N = F_G - F_{ram}$$

APPENDIX 3

Pertinent governing equations of the flight dynamic model

This appendix describes a generic, high-performance aircraft model, including detailed, full-envelope, non-linear aerodynamics. The model is a collection of interconnected modules, each performing a specific function. The primary modules of the model are aircraft actuator and surface command inputs, aircraft mass and geometry modelling, the atmospheric model and the aerodynamics, and the propulsion system and the observation variable modelling. Although the details of the model are provided in reference [**26**], the pertinent governing equations are presented in this appendix for completeness of the paper.

Aerodynamic model

The aerodynamics are modelled for the full vehicle envelope using multi-dimensional tables and linear interpolation to form non-linear function generators. In general, these aerodynamic quantities are functions of Mach number **M** and some combination of angle of attack (α), angle of sideslip (β), and symmetric stabilator deflection.

The equations defining the aerodynamic model provide non-dimensional force and moment coefficients. The longitudinal parameters are in the stability axis system; the lateral-directional parameters are given with respect to the body axis system. The equations used for this model are given in the following

$$C_L = C_{L_0} + \Delta C_{L_n} n \tag{1}$$

$$C_m = C_{m_0} + \Delta C_{m_n} n + \frac{\bar{c}}{2V}\left(C_{m_q} q + C_{m_{\dot\alpha}} \dot\alpha + C_{L_0}\Delta N_0\right) \tag{2}$$

$$C_D = C_{D_0} + \Delta C_{D_h} + \Delta C_{D_M} \tag{3}$$

$$C_y = C_{y_0} + C_{y_{\delta_A}}\delta_A + C_{y_{\delta_D}}\delta_D - \Delta C_{y_{\delta_R}}K_{\delta_{Ry}} \tag{4}$$

$$C_\ell = C_{\ell_0} + C_{\ell_{\delta_A}}\delta_A + C_{\ell_{\delta_D}}\delta_D - \Delta C_{\ell_{\delta_R}}K_{\delta_{R\ell}}$$
$$+ \frac{b}{2V}\left(C_{\ell_p} p + C_{\ell_r} r\right) \tag{5}$$

$$C_n = C_{n_0} + C_{n_{\delta_A}}\delta_A + C_{n_{\delta_D}}\delta_D$$
$$+ \Delta C_{n_{\delta_R}}K_{\delta_{Rn}} + \frac{b}{2V}\left(C_{n_p} p + C_{n_r} r\right) \tag{6}$$

Equations of motion and atmospheric model

The non-linear equations of motion used in this model are general six degree-of-freedom equations representing the flight dynamics of a rigid aircraft flying in a stationary atmosphere over a flat, non-rotating Earth. The equations for each variable in the state vector are given in the following. The following equations are used for rotational accelerations

$$\dot p = \frac{1}{\det I}[(\Sigma L)I_1 + (\Sigma M)I_2 + (\Sigma N)I_3$$
$$- p^2(I_{xz}I_2 - I_{xy}I_3) + pq(I_{xz}I_1 - I_{yz}I_2 - D_z I_3)$$
$$- pr(I_{xy}I_1 + D_y I_2 - I_{yz}I_3) + q^2(I_{yz}I_1 - I_{xy}I_3)$$
$$- qr(D_x I_1 - I_{xy}I_2 + I_{xz}I_3) - r^2(I_{yz}I_1 - I_{xz}I_2)] \tag{7}$$

$$\dot q = \frac{1}{\det I}[(\Sigma L)I_2 + (\Sigma M)I_4 + (\Sigma N)I_5$$
$$- p^2(I_{xz}I_4 - I_{xy}I_5) + pq(I_{xz}I_2 - I_{yz}I_4 - D_z I_5)$$
$$- pr(I_{xy}I_2 + D_y I_4 - I_{yz}I_5)$$
$$+ q^2(I_{yz}I_2 - I_{xy}I_5) - qr(D_x I_2 - I_{xy}I_4 + I_{xz}I_5)$$
$$- r^2(I_{yz}I_2 - I_{xz}I_4)] \tag{8}$$

$$\dot r = \frac{1}{\det I}[(\Sigma L)I_3 + (\Sigma M)I_5 + (\Sigma N)I_6$$
$$- p^2(I_{xz}I_5 - I_{xy}I_6) + pq(I_{xz}I_3 - I_{yz}I_5 - D_z I_6)$$
$$- pr(I_{xy}I_3 + D_y I_5 - I_{yz}I_6) + q^2(I_{yz}I_3 - I_{xy}I_6)$$
$$- qr(D_x I_3 - I_{xy}I_5 + I_{xz}I_6) - r^2(I_{yz}I_3 - I_{xz}I_5)] \tag{9}$$

where ΣL, ΣM, and ΣN are the aerodynamic total moments about the x-, y- and z-body axis, respectively, including power plant-induced moments, and

$$\det I = I_x I_y I_z - 2I_{xy}I_{xz}I_{yz} - I_x I_{yz}^2 - I_y I_{xz}^2 - I_z I_{xy}^2$$
$$I_1 = I_y I_z - I_{yz}^2$$
$$I_2 = I_{xy}I_z + I_{yz}I_{xz}$$
$$I_3 = I_{xy}I_{yz} + I_y I_{xz}$$
$$I_4 = I_x I_z - I_{xz}^2$$
$$I_5 = I_x I_{yz} + I_{xy}I_{xz}$$
$$I_6 = I_x I_y - I_{xy}^2$$
$$D_x = I_z - I_y$$
$$D_y = I_x - I_z$$
$$D_z = I_y - I_x$$

The following are the equations for translational accelerations

$$\dot V = \frac{1}{m}[-D\cos\beta + Y\sin\beta + X_T\cos\alpha\cos\beta$$
$$+ Y_T\sin\beta + Z_T\sin\alpha\sin\beta$$
$$- mg(\sin\theta\cos\alpha\cos\beta - \cos\theta\sin\phi\sin\beta$$
$$- \cos\theta\cos\phi\sin\alpha\cos\beta)] \tag{10}$$

$$\dot{\alpha} = \frac{1}{Vm\cos\beta}[-L + Z_{\mathrm{T}}\cos\alpha - X_{\mathrm{T}}\sin\alpha$$
$$+ mg(\cos\theta\cos\phi\cos\alpha + \sin\theta\sin\alpha)]$$
$$+ q - \tan\beta(p\cos\alpha + r\sin\alpha) \qquad (11)$$

$$\dot{\beta} = \frac{1}{Vm}[D\sin\beta + Y\cos\beta - X_{\mathrm{T}}\cos\alpha\sin\beta$$
$$+ Y_{\mathrm{T}}\cos\beta - Z_{\mathrm{T}}\sin\alpha\sin\beta$$
$$+ mg(\sin\theta\cos\alpha\sin\beta + \cos\theta\sin\phi\cos\beta$$
$$- \cos\theta\cos\phi\sin\alpha\sin\beta)] + p\sin\alpha - r\cos\alpha$$
$$(12)$$

where X_{T}, Y_{T}, and Z_{T} are thrust along the x-, y- and z-body axes, respectively, D the drag force, L the total aerodynamic lift, V the total velocity, and Y the sideforce.

The equations defining the vehicle attitude rates and Earth-relative velocities are

$$\dot{\theta} = q\cos\phi - r\sin\phi \qquad (13)$$

$$\dot{\psi} = q\sin\phi\sec\theta + r\cos\phi\sec\theta \qquad (14)$$

$$\dot{\phi} = p + q\sin\phi\tan\theta + r\cos\phi\tan\theta \qquad (15)$$

$$\dot{h} = V(\cos\beta\cos\alpha\sin\theta - \sin\beta\sin\phi\cos\theta$$
$$- \cos\beta\sin\alpha\cos\phi\cos\theta) \qquad (16)$$

$$\dot{x} = V[\cos\beta\cos\alpha\cos\theta\cos\psi$$
$$+ \sin\beta(\sin\phi\sin\theta\cos\psi - \cos\phi\sin\psi)$$
$$+ \cos\beta\sin\alpha(\cos\phi\sin\theta\cos\psi + \sin\phi\sin\psi)]$$
$$(17)$$

$$\dot{y} = V[\cos\beta\cos\alpha\cos\theta\sin\psi$$
$$+ \sin\beta(\sin\phi\sin\theta\sin\psi + \cos\phi\cos\psi)$$
$$+ \cos\beta\sin\alpha(\cos\phi\sin\theta\sin\psi - \sin\phi\cos\psi)]$$
$$(18)$$